The Response of an Idealized Atmosphere to Localized Tropical Heating: Superrotation and the Breakdown of Linear Theory

NICHOLAS J. LUTSKO[a]

Program in Atmospheric and Oceanic Sciences, Princeton University, Princeton, New Jersey

(Manuscript received 26 June 2017, in final form 15 September 2017)

ABSTRACT

An equatorial heat source mimicking the strong diabatic heating above the west Pacific is added to an idealized, dry general circulation model. For small ($<0.5\,\mathrm{K\,day^{-1}}$) heating rates the responses closely match the expectations from linear Matsuno–Gill theory, though the amplitudes of the responses increase sublinearly. This "linear" regime breaks down for larger heating rates and it is found that this is because the stability of the tropical atmosphere increases. At the same time, the equatorial winds increasingly superrotate. This superrotation is driven by stationary eddy momentum fluxes by the waves excited by the heating and is damped by the vertical advection of low-momentum air by the mean flow and, at large heating rates, by the divergence of momentum by transient eddies.

These dynamics are explored in additional experiments in which the equator-to-pole temperature gradient is varied. Very strong superrotation is produced when a large heating rate is applied to a setup with a relatively weak equator-to-pole temperature gradient, though there is no evidence that this is a case of "runaway" superrotation.

1. Introduction

The atmosphere's response to tropical heating has garnered interest from a number of different communities. For instance, it has long been known that convective heating in the west Pacific produces responses far from the heat source via teleconnections (Wallace and Gutzler 1981), and the dynamics of these teleconnections have been extensively investigated (e.g., Simmons et al. 1983; Held and Kang 1987; Sardeshmukh and Hoskins 1988; Ting and Held 1990; Ting and Hoerling 1993; Ting 1996; Hoerling et al. 1997). In a similar setting, studies of the Madden–Julian oscillation (MJO) have often focused on the way it is driven by surface latent heat flux anomalies, and contemporary theories for the dynamics of the MJO are built on older theories for the atmosphere's response to stationary tropical heat sources (Biello et al. 2007; Arnold et al. 2012; Sobel and Maloney 2012; Yang and Ingersoll 2014; Adames and Kim 2016). Finally, the planetary community has explored the response of idealized atmospheres to the large-scale (wavenumber 1) heating that would be seen on a tidally locked planet (e.g., Merlis and Schneider 2010; Showman and Polvani 2010, 2011).

In many of these studies the tropical upper atmosphere's response resembles the response of a linear shallow-water layer to equatorial heating, consisting of an equatorially trapped Kelvin wave to the east of the heating and Rossby waves propagating away from the equator to the west of the heating. This is the Matsuno–Gill model (Matsuno 1966; Gill 1980), which has been used in many studies as a starting point for interpreting the results of tropical heating experiments and has also been extended to interpret more complex tropical phenomena (e.g., Phlips and Gill 1987; Showman and Polvani 2010; Arnold et al. 2012; Sobel and Maloney 2012).

In this study the linear Matsuno–Gill theory is tested in an idealized, dry general circulation model (GCM) by adding a heat source to the model that mimics the strong diabatic heating above the west Pacific. The strength of the applied heating is varied in order to identify the parameter range over which the linear theory is, at least approximately, valid; then the strength of the heating is further increased in order to investigate how the linear theory breaks down and how the response changes in the nonlinear regime.

Denotes content that is immediately available upon publication as open access.

[a] Current affiliation: Department of Earth, Atmospheric, and Planetary Sciences, Massachusetts Institute of Technology, Cambridge, Massachusetts.

Corresponding author: Nicholas Lutsko, lutsko@princeton.edu

DOI: 10.1175/JAS-D-17-0192.1

It is found that superrotation, which can be defined as an atmospheric state in which the winds at the equator are westerly, is associated with the transition from the linear regime to the nonlinear regime. Superrotation has been seen in many previous experiments involving tropical heating (Suarez and Duffy 1992; Saravanan 1993; Hoskins et al. 1999; Kraucunas and Hartmann 2005; Norton 2006; Arnold et al. 2012; Showman and Polvani 2010, 2011) and the atmospheres of Venus, Jupiter, Saturn, and Titan are all observed to superrotate. The stratosphere also superrotates during the westerly phase of the quasi-biennial oscillation and superrotation has been linked to the ''permanent El Niño'' state of the tropical Pacific during the Pliocene (Tziperman and Farrell 2009) and may reappear in extreme global warming scenarios (Caballero and Huber 2010).

Because it is so common, there is much interest in constructing scenarios in which atmospheric models superrotate. Superrotation was initially studied in idealized, two-layer models (Suarez and Duffy 1992; Saravanan 1993) and it was found that these systems exhibit hysteresis: the equatorial winds continue to be westerly even when the heating is removed. Hysteresis is also seen in the axisymmetric shallow-water model of Shell and Held (2004).

Showman and Polvani (2010) demonstrated that a modified form of the Matsuno–Gill model fluxes momentum into the equator and hence can induce superrotation. This theory was verified in a follow-up study in which a heating mimicking that experienced by a tidally locked exoplanet was applied to an idealized, multilevel GCM (Showman and Polvani 2011). In a similar study, Kraucunas and Hartmann (2005) found that the eddy response to wavenumber-2 heating of a dry GCM, similar to the one used below, converges momentum onto the equator, producing superrotation. Analysis of the GCM's momentum budget indicated that the superrotation is limited by the vertical advection of low-momentum near-surface air by the mean tropical circulation. Strengthening the mean circulation by making the equilibrium temperature field hemispherically asymmetric eliminates the superrotation, at least for the heating rates considered by Kraucunas and Hartmann. Hoskins et al. (1999) and Norton (2006) demonstrated that the eddy response to tropical heating converges momentum into the equator in other idealized GCMs, while Arnold et al. (2012) showed that a zonally propagating heating mimicking the MJO can also produce superrotation.

With the right parameter settings, models can superrotate without a localized heat source. This is commonly seen for planets that are slowly rotating and/or have small radii, that is, those with a large (>1) ''thermal Rossby number'' (Mitchell and Vallis 2010). Wang and Mitchell (2014) recently identified a linear instability to explain this result, consisting of the interaction between a tropical Kelvin wave and Rossby waves at higher latitudes. By analyzing a combination of simulations and reanalysis data for Earth and other solar system bodies, Wang and Mitchell demonstrated that this instability is a necessary (though not sufficient) condition for superrotation in planetary atmospheres with axisymmetric forcing. In a related study, Polichtchouk and Cho (2016) found that superrotation can be generated in the presence of a weak equator-to-pole temperature gradient because of the reduction of breaking baroclinic waves from the midlatitudes and because of the presence of barotropic instability in the deep tropics. Polichtchouk and Cho also investigated the sensitivity of the superrotation to the horizontal resolution of their idealized GCM. Schneider and Liu (2009) and Liu and Schneider (2011) showed that equatorial convection on gas giants can cause superrotation by exciting Rossby waves in the deep tropics. These waves propagate to higher latitudes, where they break and transfer momentum back to their source, accelerating the equatorial winds. Finally, Laraia and Schneider (2015) developed a scaling argument for the conditions under which equatorial convection is strong enough to produce superrotation.

The experiments described below are similar to those performed by Kraucunas and Hartmann, though the horizontal extent of the heating is smaller and a much larger range of heating rates is used here. This allows the evolution of the response as a function of the heating rate to be studied in greater detail. Additional experiments are performed in which the equator-to-pole temperature gradient is varied in order to explore how this affects the response. Strong superrotation, with winds above the equator reaching over $70\,\mathrm{m\,s^{-1}}$, is produced when large heating rates are added to a setup with a relatively weak equator-to-pole temperature gradient.

The model and experiments are described in the following section, after which the results of the experiments with the original Held–Suarez setup are described in section 3 and the mechanisms responsible for the superrotation are analyzed in section 4. The effects of varying the meridional temperature gradient are discussed in sections 5 before the paper ends with conclusions in section 6.

2. Model and experiments

The GCM used in this study is the GFDL spectral dynamical core. This solves the primitive equations, forced by zonally symmetric Newtonian relaxation to a prescribed equilibrium temperature field and damped by Rayleigh friction near the surface and hyperdiffusion in the divergence equation. To start with, the parameter

TABLE 1. Experiments performed with the GCM.

Q_0 (K day^{-1})	Length (days)	Resolution	ΔT_y (K)
0	40 000, 20 000	T42, T85	40, 60, 80
0.1	40 000	T42	60
0.2	40 000, 20 000	T42, T85	40, 60, 80
0.25	40 000	T42	60
0.5	40 000, 20 000	T42, T85	40, 60, 80
0.75	20 000	T42	60
1	20 000, 20 000	T42	40, 60, 80
2	20 000, 20 000	T42, T85	40, 60, 80
3	20 000	T42	60
4	20 000, 20 000	T42, T85	40, 60, 80
5	20 000	T42	60
7.5	20 000, 20 000	T42, T85	40, 60, 80

settings are the standard Held and Suarez (1994) parameters with forcing symmetric about the equator.

The model was run at T42 resolution with 40 evenly spaced σ levels. The stronger heatings produce responses that extend into the stratosphere and, although a relatively high vertical resolution is used, the stratospheric responses are likely distorted by the even spacing of the σ levels. It is unclear how this affects the tropospheric responses.

The control simulation consisted of a 40 000-day integration, with the first 2000 days discarded and data sampled once per day. Some experiments were repeated at T85 resolution to confirm that the results are qualitatively the same at higher horizontal resolution, but the focus was on generating long integrations, rather than high-resolution integrations, so that the linear regime could be isolated within this particular model.

In the perturbation experiments an equatorial heat source was added to the temperature equation

$$\frac{\partial T}{\partial t} = \cdots - k_t(T - T_{\mathrm{eq}}) + Q, \quad (1)$$

where the first term on the right-hand side is the standard Held–Suarez forcing, with T_{eq} taking the form

$$T_{\mathrm{eq}} = \max\left\{200\,\mathrm{K}, \left[315\,\mathrm{K} - \Delta T_y \sin^2\phi - \Delta\theta_z \log\left(\frac{p}{p_0}\right)\cos^2\theta\right]\left(\frac{p}{p_0}^{\kappa}\right)\right\},$$

and the heat source being

$$Q(p,\phi,\lambda) = Q_0 \sin\left(\frac{p - p_t}{p_b - p_t}\pi\right) \times \exp\left\{-\left[\frac{\phi^2}{w_1^2} + \frac{(\lambda - \lambda_0)^2}{w_2^2}\right]\right\}, \quad (2)$$

where p, ϕ, and λ are pressure, latitude, and longitude, respectively; Q_0 is the maximum heating rate; and w_1 and w_2 are half-widths. In the standard Held–Suarez configuration ΔT_y is 60 K, $\Delta\theta_z$ is 10 K, p_0 is 1000 hPa, and $\kappa = 2/7$. We set p_t to 200 hPa, p_b to 800 hPa, w_1 to 20°, λ_0 to 150°, and w_2 to 30°. The horizontal extent of the heating was taken to mimic the region of strong diabatic heating in the west Pacific, where the maximum column-averaged heating is roughly 1.5 K day^{-1} [e.g., Fig. 8 of Held et al. (2002)].

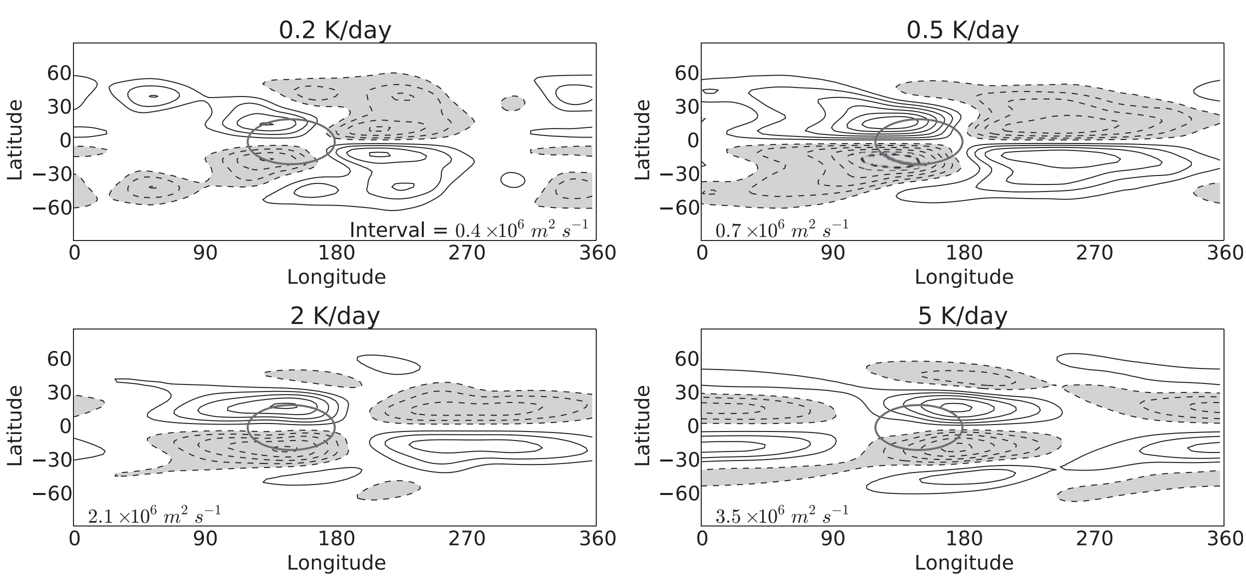

FIG. 1. Eddy streamfunction response at 350 hPa for Q_0 = (top left) 0.2, (top right) 0.5, (bottom left) 2, and (bottom right) 5 K day^{-1}. The contour intervals are given in the panels, negative values are shaded, and the green ovals show the $Q_0/2$ contour. The responses have been symmetrized about the equator to reduce the sampling error.

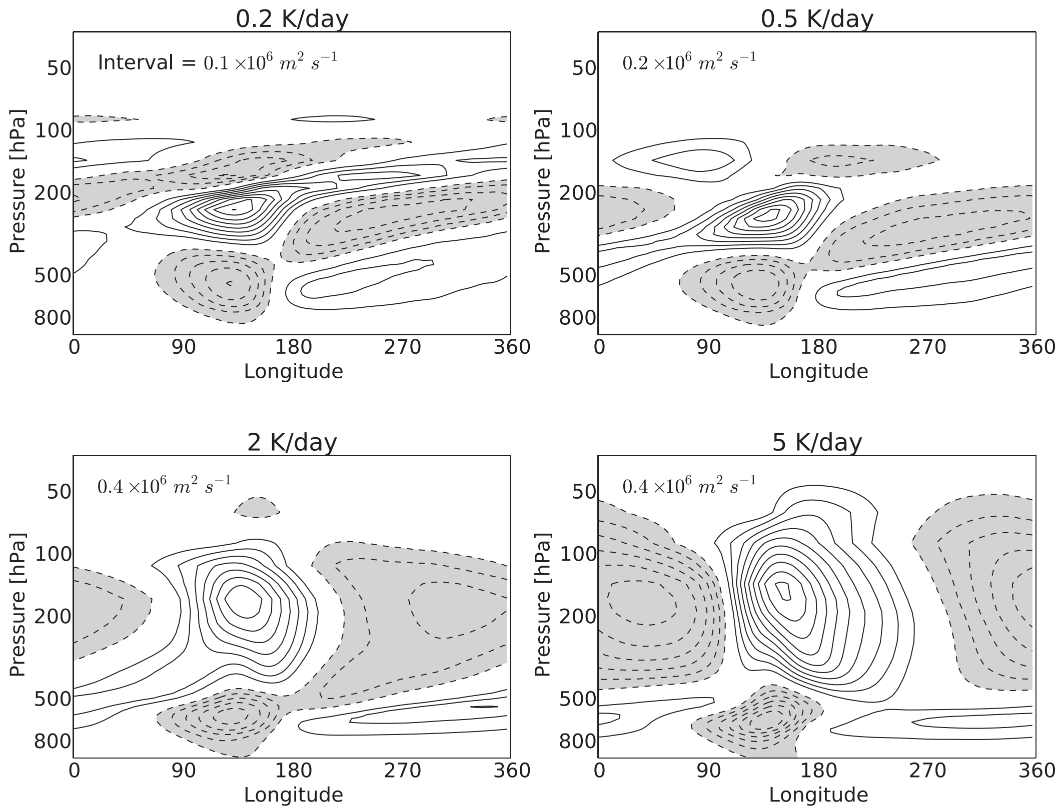

FIG. 2. Eddy streamfunction response at 2°N to equatorial heating for Q_0 = (top left) 0.2, (top right) 0.5, (bottom left) 2, and (bottom right) 5 K day^{-1}. The contour intervals are given in the panels.

The maximum heating rate Q_0 was varied from 0.1 to 7.5 K day^{-1}. The responses to smaller heating rates were not clearly separable from the noise. For comparison, the largest heating applied by Arnold et al. (2012) was 0.9 K day^{-1} and the heating applied by Kraucunas and Hartmann (2005) was 1 K day^{-1}. For heating rates less than 0.5 K day^{-1}, the responses were obtained by integrating the model for 40 000 days, discarding the first 2000 days of each experiment, and then averaging over the rest of the days. Experiments with larger heating rates were only run for 20 000 days as the responses equilibrated more quickly. A response was taken to have ''equilibrated'' when the response calculated using half of the data was indisinguishable from the response calculated using all of the data. The T85 simulations were also run for 20 000 days. A complete list of experiments is given in Table 1.

3. Responses to heating

a. *Eddy streamfunction and zonal-mean wind responses*

The top-left panel of Fig. 1 shows the eddy streamfunction response at 350 hPa for the Q_0 = 0.2 K day^{-1} experiment, with ''eddy'' referring to departures from the zonal mean. For $Q_0 < 0.5$ K day^{-1} the responses resemble that of the Matsuno–Gill model and consist of an equatorially trapped Kelvin wave and a Rossby wave in each hemisphere that propagates meridionally away from the source. The maximum response is also shifted west of the maximum heating, as predicted by linear theory. The vertical profile of the response to Q_0 = 0.2 K day^{-1} is shown in the top-left panel of Fig. 2. The response in the vicinity of the heating consists of a strong anticyclone in the upper troposphere, centered at about 250 hPa, and a weaker cyclone in the lower troposphere, centered at about 600 hPa. Away from the source, the Kelvin wave can be seen propagating with an eastward phase tilt with height, eventually extending into the stratosphere where its amplitude diminishes.

Although the amplitude of the responses increases sublinearly for heating rates less than 0.5 K day^{-1} (not shown), I will refer to these cases as being in a ''linear'' regime, as their responses have very similar patterns (not shown, but the Q_0 = 0.2 K day^{-1} case is representative) and conform with the expectations from the linear Matsuno–Gill theory. This will be made more quantitative in the next section.

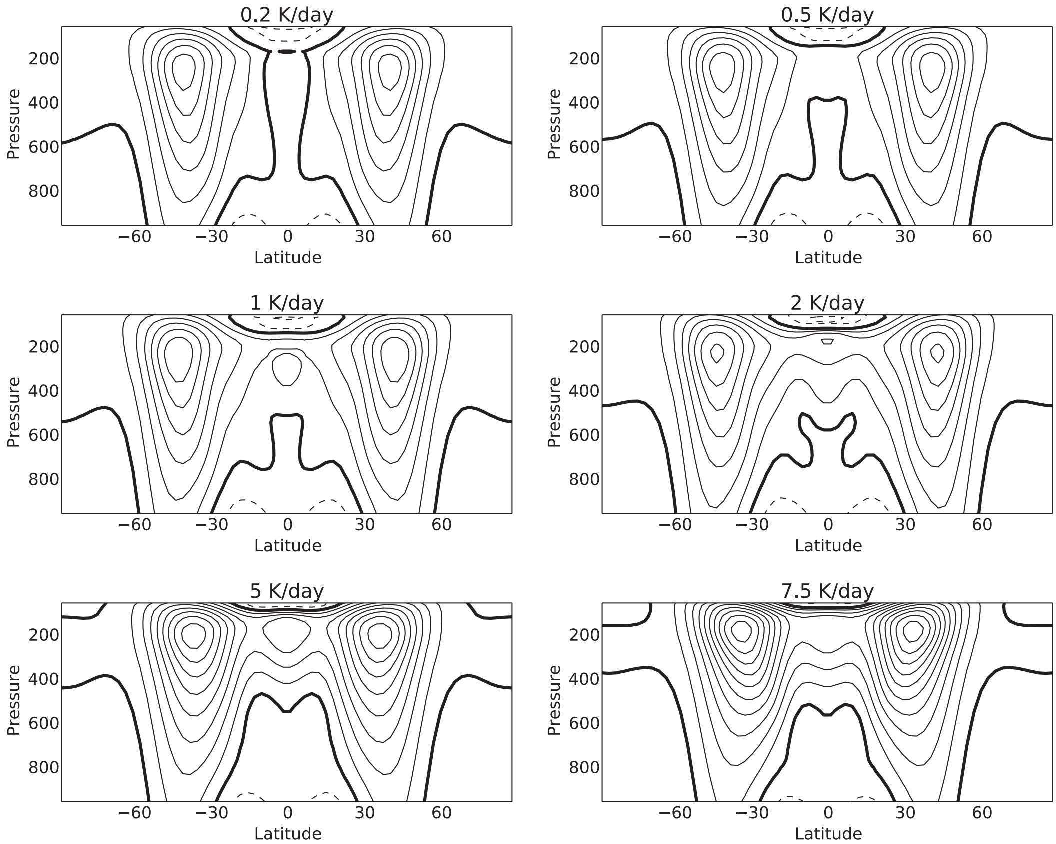

FIG. 3. Zonal-mean winds for the experiments with Q_0 = (top left) 0.2, (top right) 0.5, (middle left) 1, (middle right) 2, (bottom left) 4, and (bottom right) 7.5 K day^{-1}. In all panels the contour interval is 3 m s^{-1} and a thicker contour is used for the zero contour.

For $Q_0 = 0.5$ K day^{-1}, the Kelvin wave dominates the response at 350 hPa (top-right panel in Fig. 1), and then the Rossby wave is more prominent for larger Q_0 (bottom panels in Fig. 1). The zonal and meridional scales of the response increase with Q_0 but the normalized amplitude decreases, as can be inferred from the contour intervals. Phlips and Gill (1987) showed that if a westerly wind is added to the Matsuno–Gill model the length scales of the wave response increase. The response also shifts eastward so that its maximum is east of the maximum heating rate for large Q_0. In these cases the Rossby wave in each hemisphere propagates away from the equator along a great circle, similar to the response of a superrotating barotropic model to tropical heating seen by Sardeshmukh and Hoskins (1988). Hendon (1986) found that the response of a two-level primitive-equation model to tropical heating also shifts eastward for strong forcings.

The vertical structure of the response is similar in the 0.2 and 0.5 K day^{-1} cases, but then changes for larger Q_0 (bottom panels in Fig. 2), as the responses in the upper troposphere to these heatings consist of a wavenumber-1 wave that extends into the lower stratosphere. The maximum response is at about 175 hPa and also shifts eastward as Q_0 is increased. The response in the lower troposphere is at roughly the same height in all the experiments and does not shift in longitude, so the response in the vicinity of the heating increasingly tilts to the east with height as Q_0 is increased. The Kelvin wave is still apparent away from the forcing in the lower and midtroposphere, but it is blocked from propagating into the upper troposphere.

In addition to these eddy responses, the zonal winds at the equator increase as Q_0 is increased (Fig. 3). The flow superrotates at upper levels for $Q_0 = 0.5$ K day^{-1} and the vertically averaged winds are superrotating for $Q_0 = 1$ K day^{-1} and above, though the winds are only westerly above about 500 hPa in these experiments (bottom four panels in Fig. 3). Comparing these cases, it can be seen that a weak jet forms in the equatorial upper troposphere, but at the largest heating rate this jet is subsumed into the very strong jets in each hemisphere, which shift equatorward as Q_0 is increased (note that because of the weak Hadley circulation in the Held–Suarez setup the subtropical jets are weak).

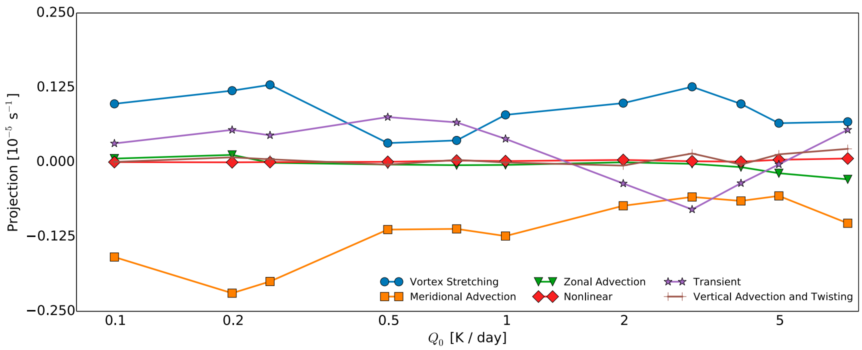

FIG. 4. Normalized projections of the terms in the stationary eddy vorticity budget onto the stationary eddy vorticity anomaly at 250 hPa, as a function of Q_0. Note the logarithmic scale for the x axis.

b. Vorticity budget analysis

Because the Coriolis force is weak in the tropics, tropical diabatic heating is primarily balanced by vertical motion acting on the static stability. This corresponds to the weak temperature gradient (WTG) approximation of the thermodynamic equation (Sobel et al. 2001)

$$\overline{\omega}^* N^2 \approx -Q, \qquad (3)$$

where the overbar denotes a time mean, the asterisk denotes a departure from the zonal mean, ω is the stationary eddy pressure velocity (dp/dt), and N^2 is the static stability. Substituting into the continuity equation

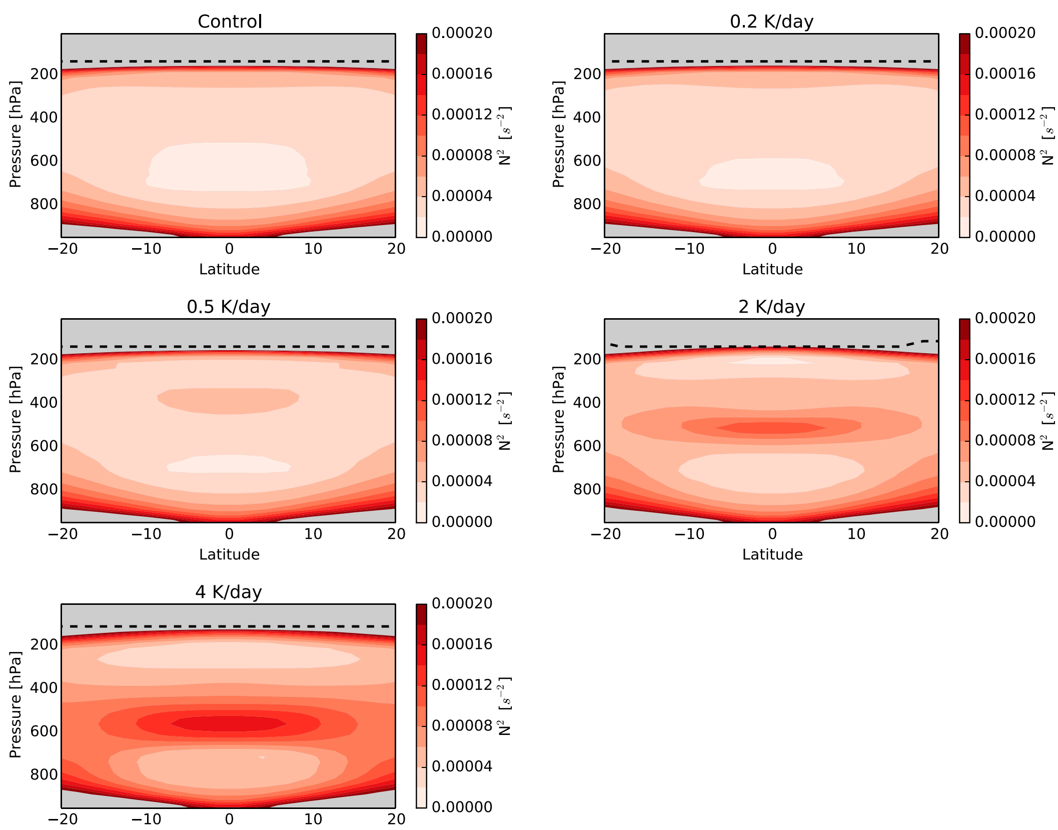

FIG. 5. Tropical static stability for (top left) the control experiment and the experiments with Q_0 = (top right) 0.2, (middle left) 0.5, (middle right) 2, and (bottom left) 4 K day^{-1}. The dashed black lines show the tropopause heights in these experiments, with the tropopause defined as the pressure at which $\partial T/\partial z < 2$ K km^{-1}. Regions in which the static stability is outside the colorbar scale are shaded in gray.

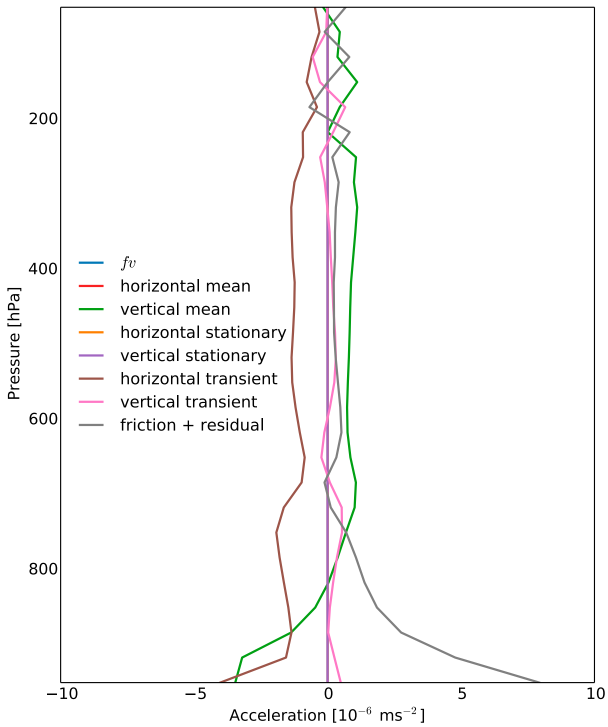

FIG. 6. Vertical profile of the zonal-momentum budget at the equator for the control experiment. The terms are defined in Eq. (8) and the text below.

then shows that heating induces a large-scale horizontal divergence

$$\nabla \cdot \overline{\mathbf{v}}^* \approx \frac{\partial}{\partial p}\left(\frac{Q}{N^2}\right), \tag{4}$$

where $\mathbf{v}$ is the horizontal velocity vector. This in turn drives rotational flow through the vortex stretching term in the stationary eddy vorticity equation

$$0 = -[\overline{u}]\frac{1}{a\cos\phi}\frac{\partial\overline{\zeta}^*}{\partial\lambda} - \left(\beta + \frac{1}{a}\frac{\partial[\overline{\zeta}]}{\partial\phi}\right)\overline{v}^* - (f + [\overline{\zeta}])\nabla\cdot\overline{\mathbf{v}}^* \\ -\nabla\cdot(\overline{\zeta}^*\overline{\mathbf{v}}^*)^* - \nabla\cdot(\overline{\zeta'\mathbf{v}'})^* - \hat{\mathbf{k}}\cdot\nabla\times\overline{\omega\frac{\partial\mathbf{v}}{\partial p}}^*, \tag{5}$$

where a is the radius of Earth, the square brackets denote a zonal mean, the prime denotes a transient term, ζ is the relative vorticity, f is the Coriolis acceleration, and β is the meridional gradient in f. The stretching term is the third term on the right-hand side. The first two terms on the right-hand side represent the linear advection of eddy vorticity by the zonal-mean zonal wind and the linear advection of mean vorticity by the eddy meridional wind, respectively. The fourth term is the nonlinear flux divergence of eddy vorticity, and the fifth term is the transient flux divergence of eddy vorticity. Finally, the sixth term is the creation of vorticity by twisting and vertical advection.

Figure 4 shows the projection of the terms in Eq. (5) onto the stationary vorticity anomaly ζ^*, normalized by the vorticity anomaly itself. That is, for a term X the projection P_X is

$$P_X = \frac{\iint \zeta^* X dA}{\iint \zeta^*\zeta^* dA}, \tag{6}$$

where A is the surface of the sphere. This quantifies the fractional contributions of the terms in the stationary vorticity budget to the stationary vorticity anomaly. The projections are taken at 250 hPa, which is a representative upper-tropospheric level (the Matsuno–Gill model is a model for the upper troposphere; the results are similar at other upper-tropospheric levels).

The Matsuno–Gill model consists of a Sverdrup balance between the second and third terms in Eq. (5), that is, between the meridional advection term and the stretching,

$$\left(\beta + \frac{1}{a}\frac{\partial[\overline{\zeta}]}{\partial\phi}\right)\overline{v}^* \sim (f + [\overline{\zeta}])\nabla\cdot\overline{\mathbf{v}}^*.$$

For $Q_0 < 0.5\,\mathrm{K\,day^{-1}}$, the perturbation is mostly driven by the stretching term and damped by the meridional advection term (Fig. 4), and so these experiments can be described as being in a "linear" regime in the sense of conforming to the linear Matsuno–Gill model. When $Q_0 = 0.5\,\mathrm{K\,day^{-1}}$, the driving by the vortex stretching decreases significantly. The meridional advection term also weakens, but not as much, and the main balance is now between this term and the transient term, which also drives the anomaly and whose contribution is relatively constant for $Q_0 < 1\,\mathrm{K\,day^{-1}}$. The contribution of the vortex stretching term increases again for larger heating rates, but the balance remains between a combination of the meridional advection, the vortex stretching, and the transient term. At the very largest heating rates the zonal advection term begins to play a role as well.

The weakening of the vortex stretching term reflects a reduction in the divergence (changes in the zonal-mean absolute vorticity are small; not shown). Laraia and Schneider (2015) give an expression for the scaling of the divergence in Eq. (4) as

$$\nabla\cdot\overline{\mathbf{v}}^* \sim \frac{gQ_0}{\theta_0 H_t N^2}, \tag{7}$$

where g is the gravitational acceleration, θ_0 is a reference potential temperature, and H_t is the tropopause height. The reduction in the divergence must arise because

H_t and/or N^2 increase, and these two quantities are shown in Fig. 5 for the control case and for four of the heating experiments. Clearly it is the static stability that causes the divergence to decrease for $Q_0 = 0.5\,\mathrm{K\,day^{-1}}$, as the heating stabilizes the tropical troposphere, while the tropopause height is essentially constant.

For small Q_0, the largest temperature change is in the upper troposphere, centered at about 300 hPa, because the stationary eddy heat flux redistributes the additional heat, shifting the largest temperature change upward from 500 hPa, where the heating is largest, in accordance with the WTG approximation [Eq. (3)]. Hence, initially, the largest stability change is also in the upper troposphere. However, as Q_0 increases the region of largest stability descends in the troposphere (Fig. 5). This also follows from the WTG: as N^2 increases in the upper troposphere the region of large ω^* (which is inversely proportional to N^2) descends in the troposphere, and so the heat flux descends also. The region of the largest temperature change thus moves lower as Q_0 increases, as does the region of highest stability.

To summarize this section, the GCM's response is in a linear regime for $Q_0 < 0.5\,\mathrm{K\,day^{-1}}$, in the sense that the dynamics conform to what is expected from the Matsuno–Gill model. For larger values of Q_0, the Sverdrup balance making up the Matsuno–Gill model breaks down as the stretching term becomes relatively weaker because of the increased stability of the tropical atmosphere and the interaction of the anomaly and the transient term in Eq. (5), which drives the stationary vorticity anomaly, becomes more prominent. At the same time, the equatorial winds begin to superrotate, breaking the assumption of the Matsuno–Gill model that the tropics are quiescent, though the linear regime breaks down before significant superrotation develops. The next section analyzes the zonal-momentum budget in order to understand the reasons for the transition to superrotation.

4. Zonal-momentum budget

The steady-state zonal-mean momentum budget is

$$\begin{aligned} 0 = f[\overline{v}] - \frac{[\overline{v}]}{a\cos\phi}\frac{\partial}{\partial\phi}([\overline{u}]\cos\phi) - [\overline{\omega}]\frac{\partial[\overline{u}]}{\partial p} - \frac{1}{a\cos^2\phi}\frac{\partial}{\partial\phi}([\overline{u}^*\overline{v}^*]\cos^2\phi) - \frac{\partial}{\partial p}[\overline{u}^*\overline{\omega}^*] \\ - \frac{1}{a\cos^2\phi}\frac{\partial}{\partial\phi}([\overline{u'v'}]\cos^2\phi) - \frac{\partial}{\partial p}[\overline{u'\omega'}] + [\overline{F_x}], \end{aligned} \tag{8}$$

where F_x is the frictional drag in the zonal direction. The vertical Coriolis term, the metric terms, and the hyperdiffusion have been ignored as they are negligible terms in the budget (not shown). I will refer to the second and third terms on the right-hand side as the mean horizontal and the mean vertical terms, respectively; the fourth and fifth terms as the stationary horizontal and stationary vertical terms, respectively; and the sixth and seventh terms as the transient horizontal and transient vertical terms, respectively.

The vertical profiles of the terms in the budget at the equator are shown for the control simulation in Fig. 6 (note that there are no grid points on the equator and so equatorial values have been obtained by averaging the values on either side of the equator). Outside of the boundary layer, the dominant balance is between the vertical advection of air by the Hadley circulation, which accelerates the flow, and the divergence of momentum by horizontally propagating transient eddies, which decelerates the flow. This is the same balance seen by Laraia and Schneider (2015).

Figure 7 shows the difference between the terms in the equatorial momentum budget for $Q_0 = 0.5\,\mathrm{K\,day^{-1}}$ and the control experiment. The changes in fv, the mean horizontal term, the transient vertical term, and the friction (outside the boundary layer) are small and so these are not shown. The stationary horizontal term transfers momentum from the subtropics into the equator, with two maxima, one at about 250 hPa and one at about 650 hPa (Fig. 7, top-left panel). These are the heights at which the eddy streamfunction response is largest (Fig. 2). The stationary vertical term cannot cause a vertical-mean acceleration of the flow (Potter et al. 2014), but it redistributes momentum vertically: there are minima at the equator close to the heights of the maxima in the stationary horizontal eddy momentum flux (EMF) and a maximum in the midtroposphere. Hence, the stationary wave transfers momentum from the subtropical upper and lower troposphere into the equatorial midtroposphere [this was also seen by Norton (2006)].

As in Kraucunas and Hartmann (2005), for this small heating rate the acceleration is opposed by the vertical mean term, which decelerates the flow by bringing up low-momentum air from near the surface. This deceleration is largest at about 350 hPa. The transients weakly decelerate the flow at about 200 hPa and accelerate the flow at lower altitudes.

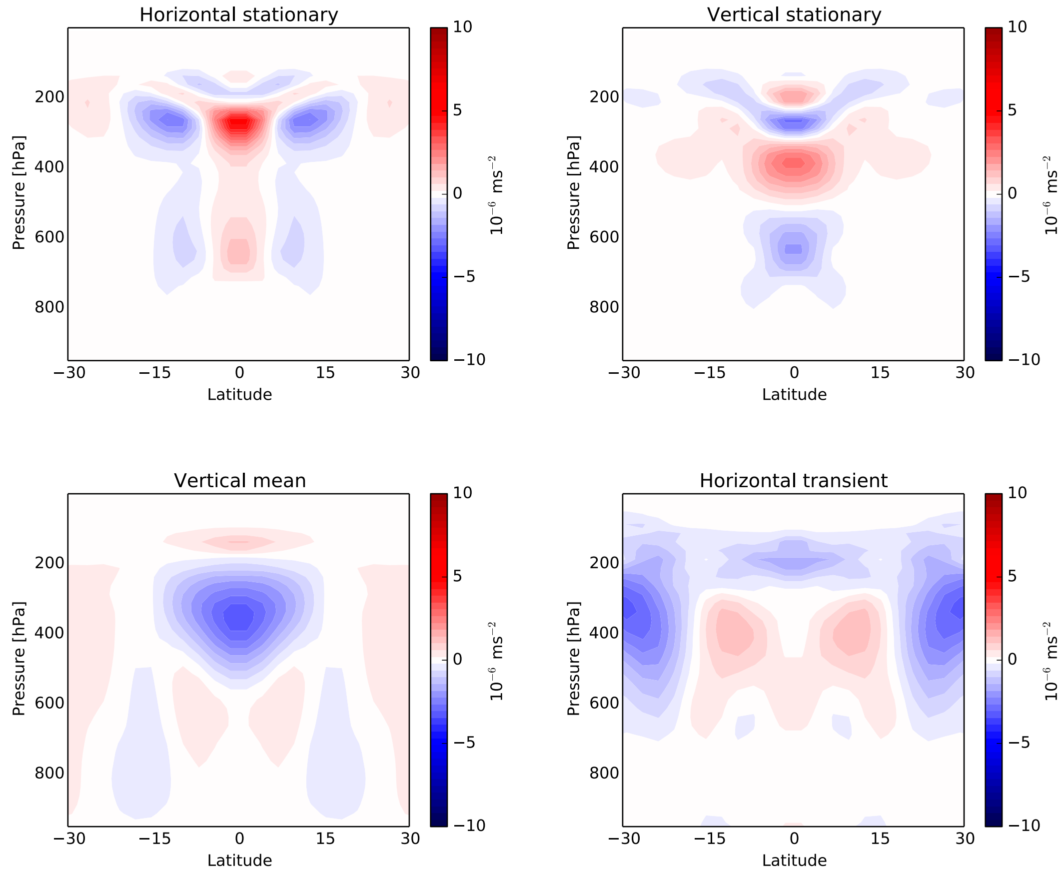

FIG. 7. Zonal-mean responses of the (top left) horizontal stationary, (top right) vertical stationary, (bottom left) vertical mean, and (bottom right) horizontal transient terms in the zonal-momentum budget for $Q_0 = 0.5\,\mathrm{K\,day^{-1}}$.

Examining the transient evolution of the zonal winds in the perturbation experiments (Fig. 8) reveals that initially the stationary wave causes a large acceleration of the equatorial winds in the midtroposphere, as the horizontal stationary flux transfers momentum into the equatorial upper and lower troposphere and the vertical stationary term transfers this to the midtroposphere. After about 40 days the mean vertical term adjusts, however, and counters the acceleration in the midtroposphere, so that the region of maximum acceleration moves to the upper troposphere.

Profiles of the responses of the terms in the equatorial momentum budget are shown for several values of Q_0 in Fig. 9, with the changes normalized by $1\,\mathrm{K\,day^{-1}}/Q_0$. The stationary horizontal EMF convergence is similar in the $Q_0 = 0.2\,\mathrm{K\,day^{-1}}$ and the $Q_0 = 0.5\,\mathrm{K\,day^{-1}}$ cases, with a sharp peak at about 250 hPa and a broader peak in the lower troposphere centered at about 650 hPa. The upper-tropospheric peak is slightly lower in the $0.5\,\mathrm{K\,day^{-1}}$ case and close inspection of Fig. 2 shows that the maximum eddy streamfunction response in this case is also at a slightly lower altitude in the upper troposphere. The upper-tropospheric peak in the stationary horizontal EMF convergence is relatively weaker for larger heating rates, though it has approximately the same normalized magnitude for $Q_0 = 2$–$7.5\,\mathrm{K\,day^{-1}}$ and is shifted up to

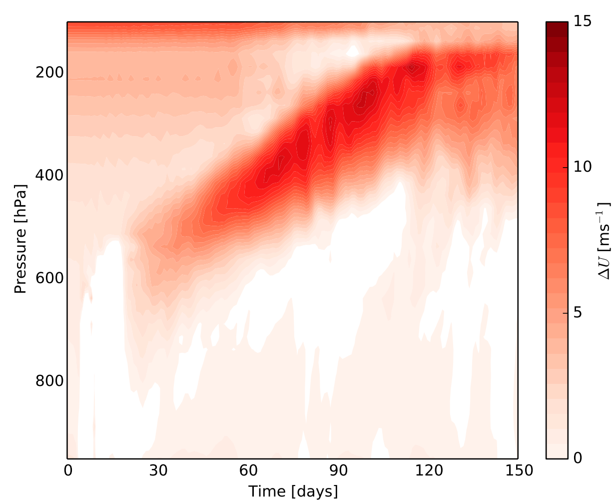

FIG. 8. Transient evolution of the response of the zonal-mean winds at the equator to the heating with $Q_0 = 0.5\,\mathrm{K\,day^{-1}}$.

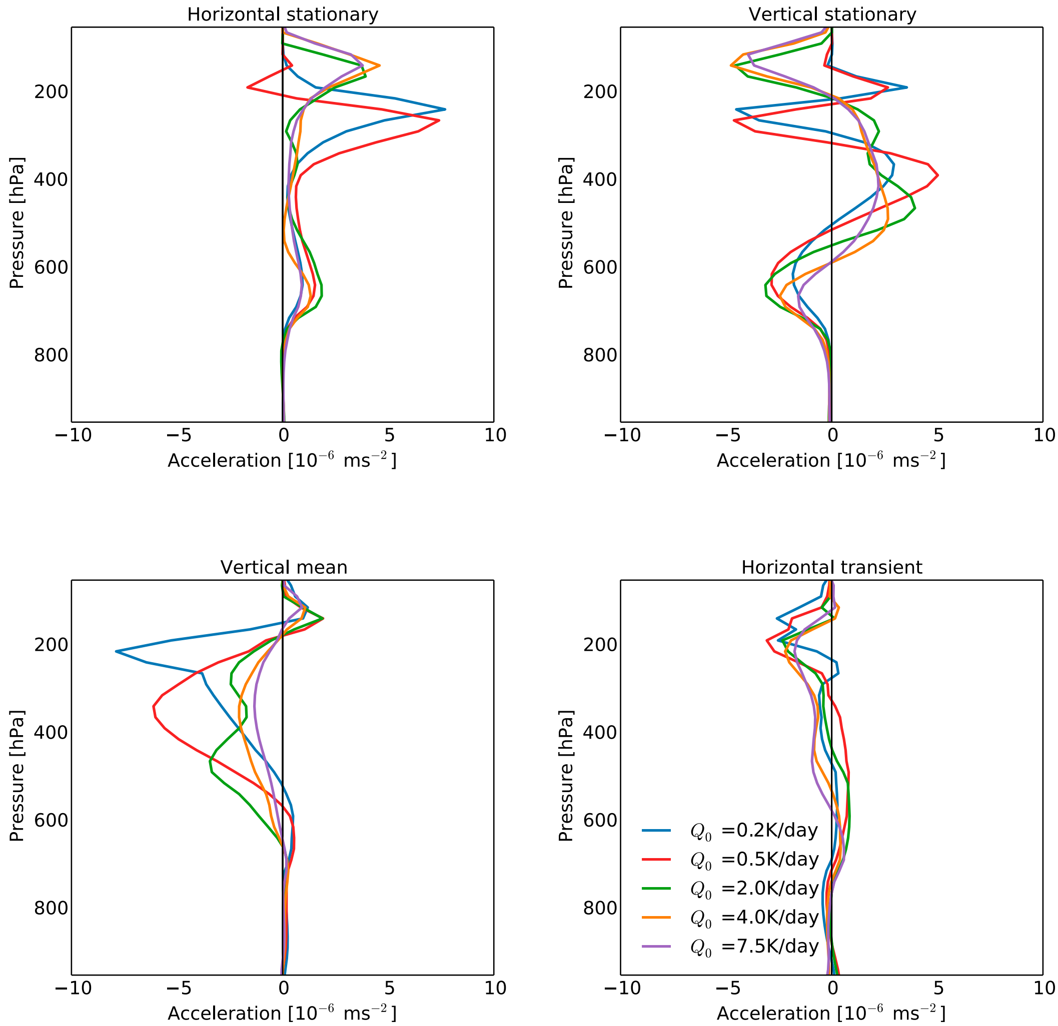

FIG. 9. Responses of the (top left) horizontal stationary, (top right) vertical stationary, (bottom left) vertical mean, and (bottom right) horizontal transient momentum fluxes at the equator to $Q_0 = 0.2$ (blue), 0.5 (red), 2 (green), 4 (orange), and 7.5 K day^{-1} (purple). The curves have been normalized by 1 K day$^{-1}/Q_0$.

about 175 hPa. This upward shift reflects the deepening of the response into the stratosphere seen in Fig. 2. In the lower troposphere the maximum stays at roughly the same height and has roughly the same normalized magnitude in all cases.

The changes of the stationary vertical term mirror those of the stationary horizontal term (top-right panel of Fig. 9). For $Q_0 = 0.2$ and 0.5 K day^{-1} the stationary vertical flux decelerates the flow between about 300 and 200 hPa and between 700 and 500 hPa, and accelerates the flow in between those levels, as well as between about 200 and 150 hPa. For the larger heatings the region of deceleration in the upper troposphere moves upward and is between about 200 and 50 hPa and the region of acceleration expands from about 600 to 200 hPa. In all of the experiments then, the stationary vertical term transfers the momentum fluxed into the equatorial upper and lower troposphere by the horizontal stationary term into the midtroposphere.

The mean vertical term is fairly similar across the different experiments, except that its normalized amplitude decreases as Q_0 is increased (bottom-left panel of Fig. 9). This is because the wind shear increases sublinearly ($[\overline{\omega}]$ does not vary substantially across the experiments; not shown). The altitude of the maximum deceleration descends as Q_0 is increased, from a sharp peak at about 200 hPa for $Q_0 = 0.2$ K day^{-1} to a smoother maximum at about 350 hPa in the larger-Q_0 experiments.

The normalized amplitude of the transient horizontal term is roughly constant and this term generally acts to decelerate the flow in the upper troposphere and accelerate the flow in the lower to midtroposphere (bottom-right

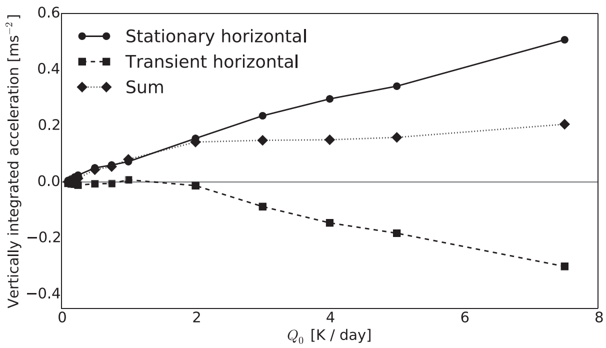

FIG. 10. Vertical integral of the equatorial stationary horizontal EMF convergence as a function of Q_0 (circles), the integral of the transient horizontal EMF convergence (squares), and the sum of the two (diamonds).

panel of Fig. 9). However, as Q_0 increases the transition from deceleration to acceleration descends, so that the transient eddies decelerate the flow more strongly in the vertical mean. This is made clearer in Fig. 10, which plots the vertical integrals of the stationary horizontal EMF convergence, the transient horizontal EMF convergence, and the sum of the two as a function of Q_0. The integral of the stationary horizontal EMF convergence increases monotonically with Q_0, though the rate of increase decreases for $Q_0 \geq 0.5\,\mathrm{K\,day^{-1}}$, while the integral of the transient horizontal term is essentially zero until $Q_0 = 2\,\mathrm{K\,day^{-1}}$, after which it increases rapidly and so the sum of these two terms is roughly constant for $Q_0 \geq 2\,\mathrm{K\,day^{-1}}$ (the sum is balanced by the vertical-mean term and the friction).

This result contrasts with previous studies, such as Kraucunas and Hartmann (2005), which have found the mean vertical term to be the only negative feedback on the superrotation. Here the mean vertical term saturates with Q_0, whereas the horizontal transient term increases for large heating rates. The transient EMF divergence increases because the acceleration of the winds in the deep tropics allows eddies originating in midlatitudes to penetrate deeper into the tropics and break closer to the equator, transferring more momentum from the deep tropics to the extratropics. This can be seen from Fig. 11, which shows the EMF cospectra at 450 hPa for the control case and for the $Q_0 = 5\,\mathrm{K\,day^{-1}}$ case. The cospectra are calculated using the standard procedure described in Hayashi (1971), Randel and Held (1991), Chen and Held (2007), and others. The 450-hPa level is chosen because this is the height of the largest changes in the EMF divergence (Fig. 9). Comparison of the control case and the case with the heating shows that eddies with slow, even westward, angular phase speeds are able to propagate much deeper into the tropics, leading to increased EMF divergence over the equator. Note that this is the opposite of what happens in the two-level model of Saravanan; in that model the tropics become entirely transparent to baroclinic eddies, which pass into the opposite hemisphere without impacting the equatorial flow.

5. Varying the baroclinicity

Stronger (weaker) baroclinicity at midlatitudes leads to stronger (weaker) transient EMFs and also to a stronger (weaker) Hadley circulation, altering the momentum balance of the GCM. To investigate how the results of the previous sections are affected by this, additional experiments were performed with the equator-to-pole temperature difference in the equilibrium temperature profile Δ_y set to 40 K and with Δ_y set to 80 K. In the original Held and Suarez setup, Δ_y is 60 K.

In the experiments with $\Delta_y = 80\,\mathrm{K}$ the responses are very similar to the original cases; however, because of the stronger Hadley circulation the vertical-mean zonal winds initially increase more slowly as Q_0 is increased (orange squares in Fig. 12). But the winds keep accelerating as Q_0 is increased and when $Q_0 = 4\,\mathrm{K\,day^{-1}}$ they are actually stronger than in the corresponding $\Delta_y = 60$-K case. A similar analysis to section 3b reveals that the tropical static stability increases more slowly in this setup as Q_0 is increased and so the stationary wave response also saturates more slowly.

When $\Delta_y = 40\,\mathrm{K}$ the equatorial winds also increase more slowly at first (black circles in Fig. 12), but then there is a small jump from about 5 to about $7\,\mathrm{m\,s^{-1}}$ between $Q_0 = 4$ and $5\,\mathrm{K\,day^{-1}}$, and then a larger jump for $Q_0 = 7.5\,\mathrm{K\,day^{-1}}$, as the winds strengthen to $32\,\mathrm{m\,s^{-1}}$.

Figure 13 studies the $7.5\,\mathrm{K\,day^{-1}}$ experiment in more detail. The top-left panel shows there are very strong jets in the subtropics of each hemisphere (the maximum wind speeds are almost $100\,\mathrm{m\,s^{-1}}$), with large shear on the poleward flanks of the jets collocated with regions of transient EMF convergence. There are three circulation cells present in the tropics of each hemisphere (top-right panel): the conventional Hadley circulation rises to about 700 hPa, then there is a countercirculation extending from about 700 to 400 hPa and then a third circulation cell above this. This three cell system develops because the rising air of the Hadley circulation is impeded by a layer of very high stability in the midtroposphere (bottom-left panel).

The bottom-right panel compares the vertically integrated terms in the equatorial momentum budget for this experiment with those from the $4\,\mathrm{K\,day^{-1}}$ experiment. As would be expected from the previous section, in the $4\,\mathrm{K\,day^{-1}}$ experiment the balance is mostly between the stationary EMF convergence, which accelerates the

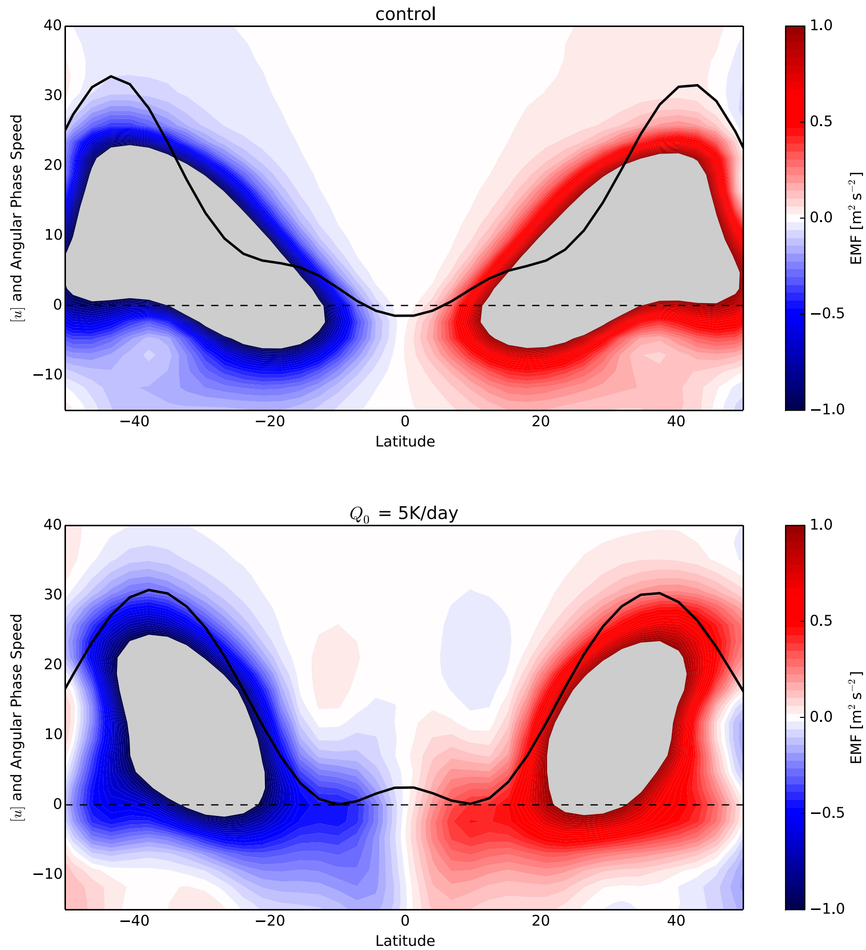

FIG. 11. EMF cospectra at the 450-hPa level in (top) the control simulation and (bottom) the $Q_0 = 5\,\mathrm{K\,day^{-1}}$ simulation. The black curves show the zonal-mean zonal winds at 450 hPa. The resolution in phase speed is $2.3\,\mathrm{m\,s^{-1}}$ and values outside the colorbar are shaded in gray.

flow, and the mean vertical advection and the transient EMF convergence, which decelerate the flow. In the $Q_0 = 7.5\,\mathrm{K\,day^{-1}}$ experiment the mean vertical advection is similar, despite the reorganization of the tropical circulation; however, the acceleration by the stationary eddies is about half the acceleration in the $4\,\mathrm{K\,day^{-1}}$ experiment, while the transient EMF convergence is almost zero. The colored contours in the top-left panel show that in the deep tropics the upper troposphere now acts as a source of transient EMF while the lower troposphere is still a sink of transient EMF, and these contributions essentially cancel when the vertical integral is taken. This is the reverse of the behavior of the transient eddies when Q_0 is small (Fig. 10), but the effect in the vertical mean is the same.

The eddy streamfunction responses near the equator in the two experiments are shown in the top panels of Fig. 14 and the vertical profiles of the stationary horizontal EMF convergence at the equator are shown in the bottom panel of this figure. The streamfunction response in the $4\,\mathrm{K\,day^{-1}}$ case is similar to the corresponding case with $\Delta_y = 60\,\mathrm{K}$, and the stationary wave acts to accelerate the flow throughout the troposphere. In contrast, the response in the $7.5\,\mathrm{K\,day^{-1}}$ experiment has an equivalent barotropic structure that is more similar to the vertical structure of midlatitude stationary waves. The profile of the stationary EMF convergence also changes, as the wave continues to accelerate the flow in the upper troposphere but decelerates the flow in the midtroposphere for $Q_0 = 7.5\,\mathrm{K\,day^{-1}}$ and so the net acceleration of the equatorial winds by the wave is reduced.

The strong superrotation is reminiscent of the axisymmetric shallow-water model results of Shell and Held (2004) and also of the two-level results of Saravanan (1993), both of which found hysteresis in their experiments. In the shallow-water model the only damping on superrotation is the vertical advection of low-momentum air by the Hadley circulation, and a

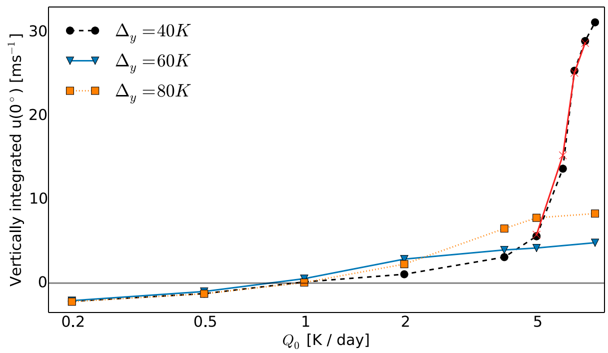

FIG. 12. Vertical-mean equatorial zonal-mean zonal wind as a function of Q_0 for $\Delta_y = 40$ (circles), 60 (triangles), and 80 K (squares). The red crosses show experiments run with $\Delta_y = 40$ K and initialized with the final state from the $Q_0 = 7.5$ K day^{-1} experiment.

hysteresis is present as the damping either weakens as the applied forcing is increased or strengthens as the forcing is increased, resulting in the existence of a strongly superrotating state and a weakly superrotating state for the same forcing (Shell and Held 2004). In the two-level model the tropics become transparent to baroclinic eddies when strong equatorial heating is applied, eliminating the damping due to the transient EMF divergence. This persists when the heating is removed and so this model also experiences hysteresis (Saravanan 1993).

While neither of these is exactly analogous to the situation here, the possibility of hysteresis in the GCM was investigated by performing a number of experiments initialized with the final state of the $Q_0 = 7.5$ K day^{-1} experiment (red crosses in Fig. 12), as well as some additional experiments starting from rest and using values of Q_0 between 5 and 7.5 K day^{-1}. No evidence of hysteresis was found, however, because the transition from the equator being a sink of baroclinic eddies to the equator being both a source and a sink of baroclinic eddies is gradual, and there is no sudden jump from one state to the other. Moreover, although the tropical circulation transitions to having a three-cell structure, the deceleration by the mean vertical advection stays roughly constant.

These additional experiments can also be used to clarify the causes of the jump in the superrotation. The

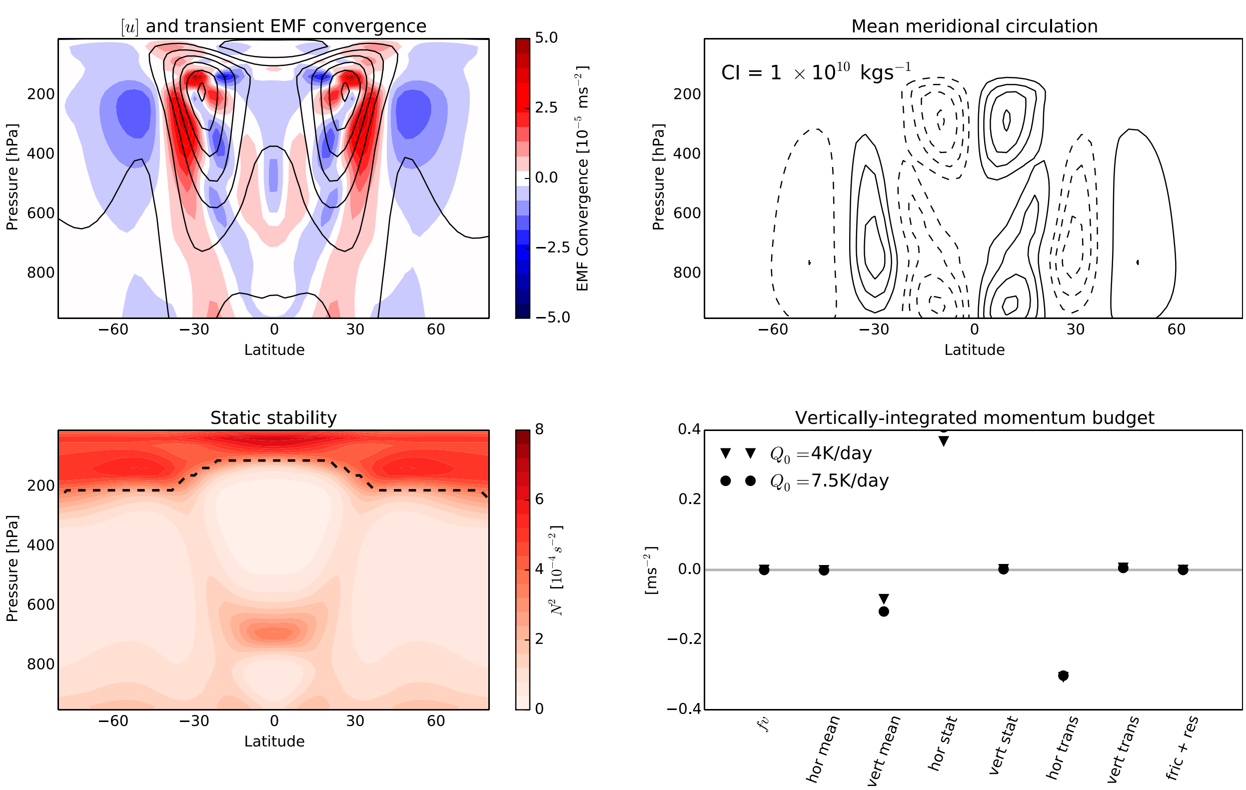

FIG. 13. (top left) Zonal-mean zonal wind (black contours; interval = 10 m s^{-1}) and eddy momentum flux convergence (colored contours) for the case with $Q_0 = 7.5$ K day^{-1} and $\Delta_y = 40$ K. (top right) As in the top-left panel, but for the mean meridional circulation. (bottom left) As in the top-left panel, but for the static stability. (bottom right) Terms in the vertically integrated momentum budget at the equator for the $Q_0 = 4$ K day^{-1} and $Q_0 = 7.5$ K day^{-1} experiments.

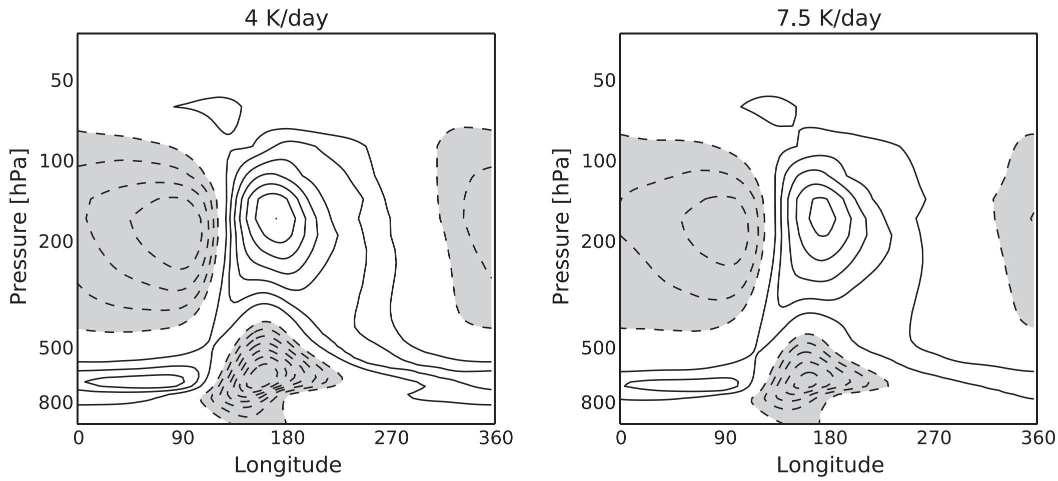

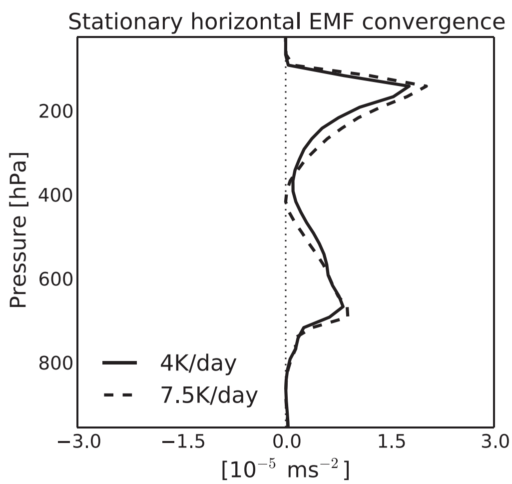

FIG. 14. The eddy streamfunction responses at 2°N for Q_0 = (top left) 4 and (top right) 7.5 K day^{-1} with Δ_y = 40 K. (bottom) The vertical profiles of the stationary horizontal EMF convergence in these experiments.

colors in Fig. 15 show the zonal-mean temperatures in the $Q_0 = 5\,\mathrm{K\,day^{-1}}$ and $Q_0 = 6\,\mathrm{K\,day^{-1}}$ cases. A region of high temperatures develops at about 650 hPa in the $Q_0 = 6\,\mathrm{K\,day^{-1}}$ case and as a result the winds in the midtroposphere also increase substantially (black contours in Fig. 15) in order to maintain thermal wind balance. The structure of the upper-tropospheric winds is quite similar in the two cases.

This explains the jump in the vertically integrated winds between the $Q_0 = 5\,\mathrm{K\,day^{-1}}$ and $Q_0 = 6\,\mathrm{K\,day^{-1}}$ cases. However, the very strong superrotation for $Q_0 = 7.5\,\mathrm{K\,day^{-1}}$ is also due to the increased EMF convergence in the upper troposphere, which is not present in the $Q_0 = 6\,\mathrm{K\,day^{-1}}$ case.

The winds in the $Q_0 = 7.5\,\mathrm{K\,day^{-1}}$ are similar to the "G" experiment in Williams (2003) in which the rotation rate of the same GCM, with a slightly different T_{eq}, was reduced to one-eighth of Earth's rate. This also produced EMF convergence in the upper-equatorial atmosphere, and Williams showed that this was caused by long, slow waves that are excited by barotropic instability. In a different parameter setting, Polichtchouk and Cho (2016) also demonstrated that barotropic instability can develop in the tropics of strongly superrotating atmospheres and that the resulting eddies flux momentum equatorward.

To investigate whether this is happening here, the quasigeostrophic potential vorticity gradient $\mathrm{PV}_\phi = f + \overline{\zeta}_y + 2\Omega\sin\phi(\overline{\theta}_y/\overline{\theta}_p)_p$ is shown in the top panel of Fig. 16. Although there is no reversal of the meridional PV gradient in the tropics, there are regions near 200 hPa and ±10° that are only marginally stable. As seen by Williams (2003), the eddies seem to successfully eliminate the barotropic instability in the time mean, but for transient periods these regions are barotropically unstable. The bottom panel of Fig. 16 shows

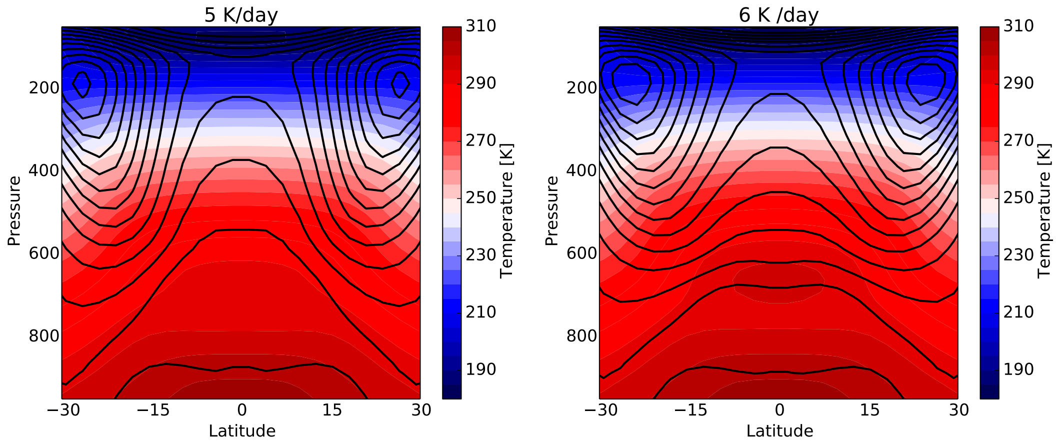

FIG. 15. Zonal-mean temperatures (colors) and zonal-mean winds (black contours) for the cases with Δ_y 40 = K and Q_0 = (left) 5 and (right) 6 K day^{-1}. The contour interval for the zonal-mean winds is 5 m s^{-1}.

the EMF cospectra at 250 hPa for the $Q_0 = 7.5$ K day^{-1} experiment; this is the height of maximum EMF convergence. The situation is clearly very different from the cases shown in Fig. 11, as the EMF convergence is due to slow, long eddies that transfer momentum into the equator. This is again similar to the situation in Williams (2003). Since the phase speeds of these waves are both positive and negative they are likely a

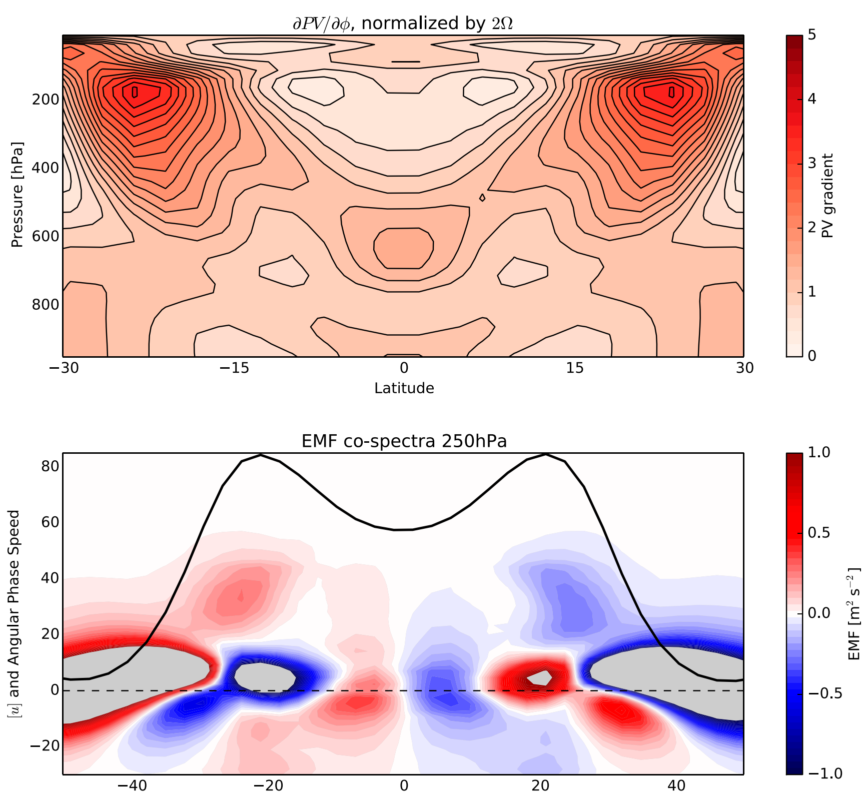

FIG. 16. (top) The zonal-mean quasigeostrophic PV gradient (PVϕ), normalized by 2Ω, in the simulation with Δ_y = 40 K and Q_0 = 7.5 K day^{-1}. (bottom) The EMF cospectra at 250 hPa in the same simulation. The black curves show the zonal-mean zonal winds at 250 hPa. The resolution in phase speed is 2.3 m s^{-1} and values outside the colorbar are shaded in gray.

combination of equatorial Rossby waves and equatorial Kelvin waves.

6. Conclusions

This study has investigated the response of a dry, idealized GCM to an equatorial heat source that mimics the convective heating over the west Pacific. Using the standard Held–Suarez setup it is found that weak ($<0.5\,\mathrm{K\,day^{-1}}$) heating rates produce responses that are in an approximately linear regime, in which the dominant vorticity balance is the Sverdrup balance of the linear Matsuno–Gill model to equatorial heating. The breakdown of the linear regime takes place because the heating stabilizes the tropical atmosphere, which causes the stretching term in the vorticity budget to increase sublinearly as Q_0 is increased, and so the transients play a more important role in driving the stationary vorticity anomaly. In the nonlinear regime, the response is dominated by a Rossby wave that propagates away from the equator along a great circle and resembles the response of a superrotating barotropic model to a tropical heat source (Sardeshmukh and Hoskins 1988).

At the same time, the model increasingly superrotates as the maximum heating rate is increased. This is a potential cause of the breakdown of the linear regime, as the Matsuno–Gill model assumes that the tropics are quiescent, but in the original setup the response becomes nonlinear because of the increased stability of the tropical troposphere before the superrotation becomes significant. Instead, the stability of the tropical atmosphere increases, reducing the driving of the stationary vorticity anomaly by the vortex stretching, but the heating affects the transient eddies in such a way that they become the main driver of the vorticity anomaly.

The superrotation is driven by the equatorward flux of momentum by the stationary waves excited by the heating and is damped by the vertical advection of low-momentum air by the mean circulation and, for larger heating rates, by the transient eddies, which increasingly break in the deep tropics, transferring momentum to higher latitudes. This contrasts with previous studies, such as Kraucunas and Hartmann (2005), in which the mean vertical advection term is the only negative feedback on superrotation. This difference reflects the much larger range of heating rates used in this study. The results here are also quite different from the idealized studies of Shell and Held (2004) and Saravanan (1993). The former assumed that the mean vertical advection was the only negative feedback on superrotation, while in the two-level model of Saravanan (1993) the equator becomes transparent to transient eddies, which propagate from one hemisphere to the other. Here transient eddies are one of the main negative feedbacks on the acceleration of the equatorial winds when strong heating is applied to the GCM.

These dynamics have been explored by varying the equator-to-pole temperature gradient of the equilibrium temperature field. The same qualitative behavior is seen in these experiments; however, the model can be made to strongly superrotate, with equatorial winds of more than $70\,\mathrm{m\,s^{-1}}$, by applying a large heating to a setup with a smaller equator-to-pole temperature gradient ($\Delta_y = 40\,\mathrm{K}$). This large acceleration occurs because the equatorial upper troposphere transitions from being a sink for transient baroclinic eddies to becoming a source of long, slow barotropic eddies. This case is very similar to the ''G'' case of Williams (2003). A region of high temperatures in the equatorial midtroposphere also causes the region of superrotation to expand vertically, in order to maintain thermal wind balance. No evidence of hysteresis was seen. Note, also, that the strong superrotation requires a maximum heating rate greater than $5\,\mathrm{K\,day^{-1}}$, which is roughly 3 times the largest heating rates observed in the present climate of Earth.

Earth's atmosphere currently seems to respond approximately linearly to the tropical heating it experiences; however, this linear regime could break down if the tropical heating on Earth were to strengthen or if the equator-to-pole temperature gradient were to be reduced significantly. Superrotation would also be more likely in these scenarios. The results of this study are also relevant for planetary atmospheres; for example, the atmosphere of a tidally locked planet that orbits close to its star would experience very strong equatorial heating. However, a major caveat is that this study has focused on the behavior of a dry atmosphere. Some of the same dynamics might be expected to hold in moist models; for instance, moist models also produce Matsuno–Gill-type responses to tropical heating (e.g., Carlson and Caballero 2016; Leroux et al. 2016), but the key differences would be in the response of the tropical stability and in the shape of the heating, which would deepen as the maximum heating rate is increased. It is left for future work to determine how the results of this study would be affected by the presence of atmospheric water vapor.

Acknowledgments. I thank Isaac Held for advice throughout this project. The manuscript was much improved by the comments of three anonymous reviewers, as well as helpful comments from Pablo Zurita-Gotor, Yi Ming, and Angel Adames. I thank the NSF for support through Grant DGE 1148900.

REFERENCES

Adames, A. F., and D. Kim, 2016: The MJO as a dispersive, convectively coupled moisture wave: Theory and observations. *J. Atmos. Sci.*, **73**, 913–941, https://doi.org/10.1175/JAS-D-15-0170.1.

Arnold, N. P., E. Tziperman, and B. Farrell, 2012: Abrupt transition to strong superrotation driven by equatorial wave resonance in an idealized GCM. *J. Atmos. Sci.*, **69**, 626–640, https://doi.org/10.1175/JAS-D-11-0136.1.

Biello, J. A., A. J. Majda, and M. W. Moncrieff, 2007: Meridional momentum flux and superrotation in the multiscale IPESD MJO model. *J. Atmos. Sci.*, **64**, 1636–1651, https://doi.org/10.1175/JAS3908.1.

Caballero, R., and M. Huber, 2010: Spontaneous transition to superrotation in warm climates simulated by CAM3. *Geophys. Res. Lett.*, **37**, L11701, https://doi.org/10.1029/2010GL043468.

Carlson, H., and R. Caballero, 2016: Enhanced MJO and transition to superrotation in warm climates. *J. Adv. Model. Earth Syst.*, **8**, 304–318, https://doi.org/10.1002/2015MS000615.

Chen, G., and I. M. Held, 2007: Phase speed spectra and the recent poleward shift of Southern Hemisphere surface westerlies. *Geophys. Res. Lett.*, **34**, L21805, https://doi.org/10.1029/2007GL031200.

Gill, A. E., 1980: Some simple solutions for heat-induced tropical circulation. *Quart. J. Roy. Meteor. Soc.*, **106**, 447–462, https://doi.org/10.1002/qj.49710644905.

Hayashi, Y., 1971: A generalized method of resolving disturbances into progressive and retrogressive waves by space Fourier and time cross-spectral analyses. *J. Meteor. Soc. Japan*, **49**, 125–128, https://doi.org/10.2151/jmsj1965.49.2_125.

Held, I. M., and I.-S. Kang, 1987: Barotropic models of the extratropical response to El Niño. *J. Atmos. Sci.*, **44**, 3576–3586, https://doi.org/10.1175/1520-0469(1987)044<3576:BMOTER>2.0.CO;2.

——, and M. J. Suarez, 1994: A proposal for the intercomparison of the dynamical cores of atmospheric general circulation models. *Bull. Amer. Meteor. Soc.*, **75**, 1825–1830, https://doi.org/10.1175/1520-0477(1994)075<1825:APFTIO>2.0.CO;2.

——, M. Ting, and H. Wang, 2002: Northern winter stationary waves: Theory and modeling. *J. Climate*, **15**, 2125–2144, https://doi.org/10.1175/1520-0442(2002)015<2125:NWSWTA>2.0.CO;2.

Hendon, H. H., 1986: The time-mean flow and variability in a nonlinear model of the atmosphere with tropical diabatic forcing. *J. Atmos. Sci.*, **43**, 72–88, https://doi.org/10.1175/1520-0469(1986)043<0072:TTMFAV>2.0.CO;2.

Hoerling, M. P., A. Kumar, and M. Zhong, 1997: El Niño, La Niña, and the nonlinearity of their teleconnections. *J. Climate*, **10**, 1769–1786, https://doi.org/10.1175/1520-0442(1997)010<1769:ENOLNA>2.0.CO;2.

Hoskins, B., R. Neale, M. Rodwell, and G. Y. Yang, 1999: Aspects of the large-scale tropical atmospheric circulation. *Tellus*, **51A**, 33–44, https://doi.org/10.3402/tellusa.v51i1.12287.

Kraucunas, I., and D. L. Hartmann, 2005: Equatorial superrotation and the factors controlling the zonal-mean zonal winds in the tropical upper troposphere. *J. Atmos. Sci.*, **62**, 371–389, https://doi.org/10.1175/JAS-3365.1.

Laraia, A. L., and T. Schneider, 2015: Superrotation in terrestrial atmospheres. *J. Atmos. Sci.*, **72**, 4281–4296, https://doi.org/10.1175/JAS-D-15-0030.1.

Leroux, S., and Coauthors, 2016: Inter-model comparison of subseasonal tropical variability in aquaplanet experiments: Effect of a warm pool. *J. Adv. Model. Earth Syst.*, **8**, 1526–1551, https://doi.org/10.1002/2016MS000683.

Liu, J., and T. Schneider, 2011: Convective generation of equatorial superrotation in planetary atmospheres. *J. Atmos. Sci.*, **68**, 2742–2756, https://doi.org/10.1175/JAS-D-10-05013.1.

Matsuno, T., 1966: Quasi-geostrophic motions in the equatorial area. *J. Meteor. Soc. Japan*, **44**, 25–42, https://doi.org/10.2151/jmsj1965.44.1_25.

Merlis, T. M., and T. Schneider, 2010: Atmospheric dynamics of Earth-like tidally locked aquaplanets. *J. Adv. Model. Earth Syst.*, **2**, 13, https://doi.org/10.3894/JAMES.2010.2.13.

Mitchell, J. L., and G. K. Vallis, 2010: The transition to superrotation in terrestrial atmospheres. *J. Geophys. Res.*, **115**, E12008, https://doi.org/10.1029/2010JE003587.

Norton, W., 2006: Tropical wave driving of the annual cycle in tropical tropopause temperatures. Part II: Model results. *J. Atmos. Sci.*, **63**, 1420–1431, https://doi.org/10.1175/JAS3698.1.

Phlips, P. J., and A. E. Gill, 1987: An analytic model of the heat-induced tropical circulation in the presence of a mean wind. *Quart. J. Roy. Meteor. Soc.*, **113**, 213–236, https://doi.org/10.1002/qj.49711347513.

Polichtchouk, I., and J. Cho, 2016: Equatorial superrotation in Held and Suarez like flows with weak equator-to-pole surface temperature gradient. *Quart. J. Roy. Meteor. Soc.*, **142**, 1528–1540, https://doi.org/10.1002/qj.2755.

Potter, S. F., G. K. Vallis, and J. L. Mitchell, 2014: Spontaneous superrotation and the role of Kelvin waves in an idealized dry GCM. *J. Atmos. Sci.*, **71**, 596–614, https://doi.org/10.1175/JAS-D-13-0150.1.

Randel, W. J., and I. M. Held, 1991: Phase speed spectra of transient eddy fluxes and critical layer absorption. *J. Atmos. Sci.*, **48**, 688–697, https://doi.org/10.1175/1520-0469(1991)048<0688:PSSOTE>2.0.CO;2.

Saravanan, R., 1993: Equatorial superrotation and maintenance of the general circulation in two-level models. *J. Atmos. Sci.*, **50**, 1211–1227, https://doi.org/10.1175/1520-0469(1993)050<1211:ESAMOT>2.0.CO;2.

Sardeshmukh, P. D., and B. J. Hoskins, 1988: The generation of global rotational flow by steady idealized tropical divergence. *J. Atmos. Sci.*, **45**, 1228–1251, https://doi.org/10.1175/1520-0469(1988)045<1228:TGOGRF>2.0.CO;2.

Schneider, T., and J. Liu, 2009: Formation of jets and equatorial superrotation on Jupiter. *J. Atmos. Sci.*, **66**, 579–601, https://doi.org/10.1175/2008JAS2798.1.

Shell, K. M., and I. M. Held, 2004: Abrupt transition to strong superrotation in an axisymmetric model of the upper troposphere. *J. Atmos. Sci.*, **61**, 2928–2935, https://doi.org/10.1175/JAS-3312.1.

Showman, A. P., and L. M. Polvani, 2010: The Matsuno-Gill model and equatorial superrotation. *Geophys. Res. Lett.*, **37**, L18811, https://doi.org/10.1029/2010GL044343.

——, and ——, 2011: Equatorial superrotation on tidally locked exoplanets. *Astrophys. J.*, **738**, 71, https://doi.org/10.1088/0004-637X/738/1/71.

Simmons, A. J., J. M. Wallace, and G. W. Branstator, 1983: Barotropic wave propagation and instability, and atmospheric teleconnection patterns. *J. Atmos. Sci.*, **40**, 1363–1392, https://doi.org/10.1175/1520-0469(1983)040<1363:BWPAIA>2.0.CO;2.

Sobel, A., and E. Maloney, 2012: An idealized semi-empirical framework for modeling the Madden–Julian oscillation. *J. Atmos. Sci.*, **69**, 1691–1705, https://doi.org/10.1175/JAS-D-11-0118.1.

——, J. Nilsson, and L. M. Polvani, 2001: The weak temperature gradient approximation and balanced tropical moisture waves. *J. Atmos. Sci.*, **58**, 3650–3665, https://doi.org/10.1175/1520-0469(2001)058<3650:TWTGAA>2.0.CO;2.

Suarez, M. J., and D. G. Duffy, 1992: Terrestrial superrotation: A bifurcation of the general circulation. *J. Atmos. Sci.*, **49**, 1541–1554, https://doi.org/10.1175/1520-0469(1992)049<1541:TSABOT>2.0.CO;2.

Ting, M. F., 1996: Steady linear response to tropical heating in barotropic and baroclinic models. *J. Atmos. Sci.*, **53**, 1698–1709, https://doi.org/10.1175/1520-0469(1996)053<1698:SLRTTH>2.0.CO;2.

——, and I. M. Held, 1990: The stationary wave response to a tropical SST anomaly in an idealized GCM. *J. Atmos. Sci.*, **47**, 2546–2566, https://doi.org/10.1175/1520-0469(1990)047<2546:TSWRTA>2.0.CO;2.

——, and M. P. Hoerling, 1993: Dynamics of stationary wave anomalies during the 1986/87 El Niño. *Climate Dyn.*, **9**, 147–164, https://doi.org/10.1007/BF00209751.

Tziperman, E., and B. Farrell, 2009: The Pliocene equatorial temperature: Lessons from atmospheric superrotation. *Paleoceanography*, **24**, PA1101, https://doi.org/10.1029/2008PA001652.

Wallace, J. M., and D. S. Gutzler, 1981: Teleconnections in the geopotential height field during the Northern Hemisphere winter. *Mon. Wea. Rev.*, **109**, 784–812, https://doi.org/10.1175/1520-0493(1981)109<0784:TITGHF>2.0.CO;2.

Wang, P., and J. L. Mitchell, 2014: Planetary ageostrophic instability leads to superrotation. *Geophys. Res. Lett.*, **41**, 4118–4126, https://doi.org/10.1002/2014GL060345.

Williams, G. P., 2003: Barotropic instability and equatorial superrotation. *J. Atmos. Sci.*, **60**, 2136–2152, https://doi.org/10.1175/1520-0469(2003)060<2136:BIAES>2.0.CO;2.

Yang, D., and A. P. Ingersoll, 2014: A theory of the MJO horizontal scale. *Geophys. Res. Lett.*, **41**, 1059–1064, https://doi.org/10.1002/2013GL058542.